Characterisation by ^{1}H NMR spectroscopy of enzymically derived oligosaccharides from alkali-extractable wheat-flour arabinoxylan

Harry Gruppen [a], Rainer A. Hoffmann [b], Felix J.M. Kormelink [a], Alphons G.J. Voragen [a], Johannis P. Kamerling [b] and Johannes F.G. Vliegenthart [b]

[a] *Department of Food Science, Agricultural University, P.O. Box 8129, 6700 EV Wageningen (Netherlands)*
[b] *Bijvoet Center, Department of Bio-Organic Chemistry, Utrecht University, P.O. Box 80075, 3508 TB Utrecht (Netherlands)*

ABSTRACT

Oligosaccharides obtained from alkali-extractable wheat-flour arabinoxylans by digestion with endo-$(1 \rightarrow 4)$-β-D-xylanase from *Aspergillus awamori* were fractionated by size-exclusion chromatography on Bio-Gel P-2 followed by high-performance anion-exchange chromatography, and subjected to monosaccharide analysis and ^{1}H NMR spectroscopy. The results revealed $(1 \rightarrow 4)$-linked β-D-xylopyrano-oligosaccharides partly 3- and/or 2,3-substituted with single α-L-arabinofuranosyl groups. The structures of 12 such arabinoxylan oligosaccharides were established.

INTRODUCTION

Wheat-flour arabinoxylans consist[1,2] of a linear backbone of $(1 \rightarrow 4)$-β-D-xylopyranosyl residues, with mainly single α-L-arabinofuranosyl groups attached through positions 2 and 3, but little is known about the distribution of the side chains. Periodate-oxidation studies[3,4] indicated the presence of clusters of 1–4 contiguous branched β-D-Xyl$p$ residues. However, a study of water-soluble rye arabinoxylans[5] favours small isolated clusters of singly and doubly branched residues. Enzymic hydrolysis of the cell-wall material from bamboo and graminaceous plants yielded di-, tri-, and tetra-saccharides, some of which were feruloylated[6–11].

Detailed ^{1}H NMR studies of arabinoxylan oligosaccharides, derived from a warm-water-extractable arabinoxylan fraction by digestion with an *Aspergillus*

Correspondence to: Professor A.G.J. Voragen, Department of Food Science, Agricultural University, P.O. Box 8129, 6700 EV Wageningen, Netherlands.

endo-(1 → 4)-β-D-xylanase, have been reported[12,13]. The structures of alkali-extractable arabinoxylans have been less well characterised, due to the difficulties in their purification. We have described the isolation[14] of highly purified, water-unextractable, alkali-extractable arabinoxylans from wheat flour, which were further characterised[15] and fractionated by anion-exchange chromatography[16]. We now report on the structures of oligosaccharides derived from these arabinoxylans by digestion with endo-(1 → 4)-β-D-xylanase I from *Aspergillus awamori* CMI 142717, the specificity of which is different from that of the endo-(1 → 4)-β-D-xylanase previously used[12,13].

EXPERIMENTAL

Materials. —Wheat alkali-extractable arabinoxylan (BE1-U) was prepared from water-unextractable cell-wall material of the soft-wheat variety *Arminda*[15,16]. Endo-(1 → 4)-β-D-xylanase I was purified[17] from *Aspergillus awamori* CMI 142717.

Preparation of arabinoxylan oligosaccharides. —A solution of wheat alkali-extractable arabinoxylan (80 mg) in 50 mM sodium acetate buffer (80 mL, pH 5.0) was incubated with endo-(1 → 4)-β-D-xylanase I (0.4 μg/mL) for 24 h at 30°. After inactivation of the enzyme (10 min, 100°), the solution was concentrated to 3 mL under reduced pressure, and applied to a column (100 × 2.6 cm) of Bio-Gel P-2 (200–400 mesh, Bio-Rad) at 60° and eluted with distilled water (17 mL/h). Fractions (2.4 mL) were assayed for total neutral sugar content[18]. Appropriate fractions were combined, designated *1–13*, and each was concentrated to 1.5 mL under reduced pressure. The column was calibrated using a mixture of xylose, maltose, raffinose, stachyose, and Dextran T150 (Pharmacia). The elution volumes of these compounds corresponds with those of fractions *1–4*, and *13* (void), respectively.

Fractions *3–10* were subjected to high-performance anion-exchange chromatography (HPAEC), using a Dionex Bio-LC GPM-II quaternary gradient module equipped with a Dionex CarboPac PA-1 column (250 × 9 mm). Samples (5 × 300 μL) were injected using a Spectra Physics SP8780 autosampler equipped with a Tefzel rotor seal in a 7010 Rheodyne injector valve. Elution (5 mL/min) involved linear gradients of sodium acetate in 0.1 M NaOH 0 → 150 mM during 10 min, then 150 → 500 mM during 30 min at 20°. The solvents were degassed and stored under helium, using a Dionex EDM module. The eluate was monitored by using a Dionex PED detector in the pulsed-amperometric detection (PAD) mode. A reference Ag/AgCl electrode was used with a working Au electrode, with the following pulse potentials and durations: E_1 0.1 V and 0.5 s, E_2 0.6 V and 0.1 s, E_3 −0.6 V and 0.1 s. The eluate was neutralised with M acetic acid and the appropriate fractions (1.2 mL) were combined, desalted using columns (30 × 80 mm) of Dowex 50W-X8 (H$^+$) and AG3 X4A (HO$^-$) resins (Bio-Rad) in series, and concentrated under reduced pressure, and the residue was air-dried.

Monosaccharide analysis. —Samples (30–70 μg) were hydrolysed by 2 M trifluoroacetic acid for 1 h at 121°, and the acid was evaporated in a stream of air at 40°. For Bio-Gel P-2 fractions, each monosaccharide mixture was reduced in 1.5 M ammonia (0.2 mL) containing 75 mg of $NaBH_4$/mL, and the products were converted into their alditol acetates[19] and analysed[20]. *myo*-Inositol was used as internal standard. For Dionex fractions, each hydrolysate was dissolved in water and analysed on a CarboPac PA-1 column (250 × 4 mm), eluted (1 mL/min) with 0.1 M NaOH, using PAD analysis (as described above).

FABMS. —Positive-ion FAB-mass spectra were recorded with a Jeol JMS AX 505 W spectrometer (Xe beam of 6 kV, acceleration potential of 3 kV) equipped with an HP9000 data system. Each sample was dispersed in a glycerol matrix, and the mass range was scanned at 10 s/scan with a mass resolution of 1500.

^{1}H NMR spectroscopy. —Samples were repeatedly treated with D_2O (99.9 atom% D, MSD Isotopes), finally using 99.96 atom% D at pD ≥ 7. Resolution-enhanced 600-MHz ^{1}H NMR spectra were recorded with a Bruker AM-600 spectrometer (SON-hf-NMR facility, Department of Biophysical Chemistry, Nijmegen University, Netherlands), operating at a probe temperature of 27°. Chemical shifts (δ) are expressed in ppm and were measured by reference to internal acetone (δ 2.225 in D_2O at 27°)[21]. Full details of the HOHAHA spin-lock experiments and ROESY spectroscopy have been reported[12].

RESULTS AND DISCUSSION

The fractionation of the arabinoxylan digest on Bio-Gel P-2 is shown in Fig. 1, and the monosaccharide composition and yield of each combined fraction are given in Table I. Of the 13 fractions, 11 (*1–10* and *13*) were observed as separate peaks, *13* was eluted in the void volume, and *1–10* accounted for 72% of the arabinoxylan. Fractions *1* and *2*, consisting of xylose only (Table I), each showed one peak in HPAEC, and are suggested to contain xylose and xylobiose, respectively.
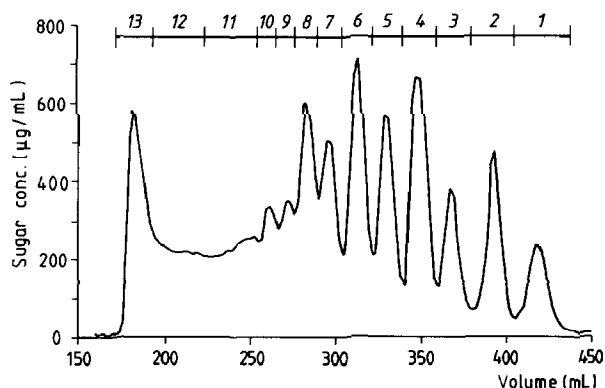

Fig. 1. Elution profile of the arabinoxylan digest on Bio-Gel P-2.

TABLE I

Data on the fractions obtained by chromatography on Bio-Gel P-2 and Dionex of the products formed by the enzymic degradation of wheat arabinoxylan

Bio-Gel P-2 fractions

	1	2	3	4	5	6	7	8	9	10	11	12	13
Yield (%)[a]	4.4	6.9	6.6	10.6	8.4	11.1	7.7	8.9	4.1	3.9	8.8	8.3	10.9
Ara (%)[b]	0	0	25	25	39	33	40	40	40	42	44	47	50
Xyl (%)	100	100	75	75	61	67	60	60	60	58	56	53	50

Dionex sub-fractions of 3–10

	3.1	3.2	4.1	5.1	5.2	6.1	6.2	6.3	7.1	8.1	8.2	9.1	9.2	10.1
Recovery (%)[c]	31	68	98	48	44	60	27	12	85	53	28	64	27	47
Ara (%)	0	33	26	38	39	35	33	46	42	40	50	43	43	38
Xyl (%)	100	67	74	62	61	65	67	54	58	60	50	57	57	62
Mol wt[d]	414	414	546	678	678	810	810	810	942	1074	1074	1206	1074 1206	1338
	(3)	(3)	(4)	(5)	(5)	(6)	(6)	(6)	(7)	(8)	(8)	(9)	(8,9)	(10)

[a] Percentage of total neutral sugars present in each fraction, based on spectrophotometric response of all sugars. [b] Sugar composition of the material in each peak. [c] Percentage of total PAD response from each Bio-Gel P-2 fraction. [d] Determined by positive-ion FABMS (number of pentose units in brackets).
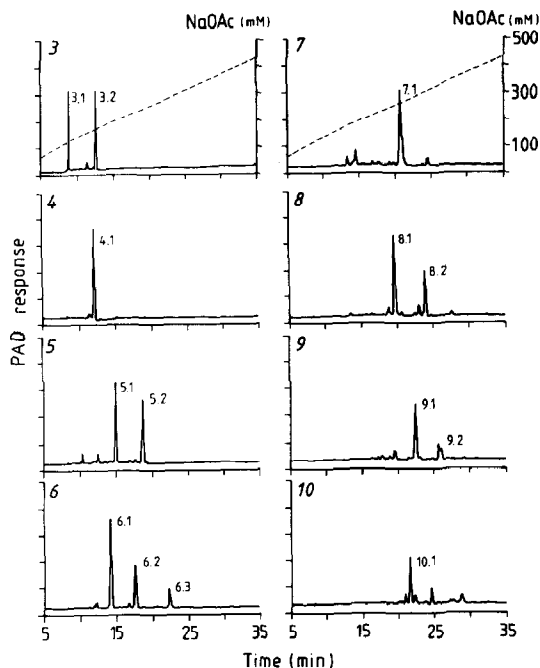
Fig. 2. Elution profile on HPAEC of Bio-Gel P-2 fractions *3–10* in Fig. 1.

Fractions *3–10* were subjected to HPAEC and the results are shown in Fig. 2. The monosaccharide compositions, molecular weights of the major components, and the recoveries are given in Table I. For fractions *4* and *7*, no further fractionation was achieved, and fractions **4.1** and **7.1** represent 98 and 85%, respectively, of the total PAD responses. Fractions *3*, *5*, *8*, and *9* each contained two major components, which represented > 90% of each total PAD response. Fraction *6* contained three oligosaccharides (**6.1**, **6.2**, and **6.3**) in the proportions 60, 27, and 12%, respectively. Fraction *10* contained one major component (47% of the total PAD response) and no attempt was made to isolate the minor components. The structures of the major oligosaccharides were elucidated by ^{1}H NMR spectroscopy.

Fraction **3.1**.—The ^{1}H NMR spectrum of **3.1** matched exactly that of the reference compound **Xyl$_3$** [β-D-Xyl$p$-(1 → 4)-β-D-Xyl$p$-(1 → 4)-D-Xyl$p$][12] and the chemical shifts of the H-1 resonances are summarised in Table II.

$$\begin{array}{ccc} 3 & 2 & 1 \end{array}$$
β-Xyl$p$-(1 → 4)-β-Xyl$p$-(1 → 4)-Xyl$p$
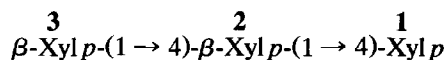
3.1

Fraction **3.2**.—The intensities of the H-1 signals for **3.2** (Fig. 3) indicated an arabinosylxylobiose structure with the Xyl$p$ units β ($J_{1,2}$ 7–8 Hz) and the Ara$f$ unit α ($J_{1,2}$ ~ 1.6 Hz)[6,22]. By comparison with published ^{1}H NMR data for the

TABLE II

Chemical shifts [a] of the H-1 resonances of fractions **3.1**, **6.1**, **8.1**, **9.1**, and **10.1** from Table I

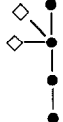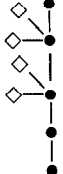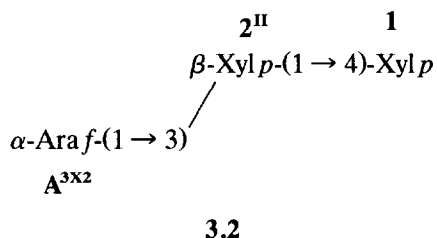| Residue [b]	3.1 [c]	6.1	8.1	9.1	10.1
α-Xyl$p$-1	5.184	5.184	5.184	5.183	5.184
β-Xyl$p$-1	4.584	4.584	4.584	4.584	4.584
β-Xyl$p$-2$_\alpha$	4.475	4.465	4.465	4.464	4.465
β-Xyl$p$-2$_\beta$	4.479	4.468	4.468	4.467	4.468
β-Xyl$p$-3	4.461				
β-Xyl$p$-3$^{\mathrm{III}}$		4.639	4.637	4.628	4.639
β-Xyl$p$-4		4.437			4.443
β-Xyl$p$-4$^{\mathrm{II}}$			4.480		
β-Xyl$p$-4$^{\mathrm{III}}$				4.578	
β-Xyl$p$-5			4.435	4.428	
β-Xyl$p$-5$^{\mathrm{III}}$					4.628
β-Xyl$p$-6					4.436
α-Ara$f$-A$^{2\mathrm{X}3}$		5.225	5.225	5.222	5.224
α-Ara$f$-A$^{3\mathrm{X}3}$		5.274	5.270	5.293	5.271
α-Ara$f$-A$^{2\mathrm{X}4}$				5.242	
α-Ara$f$-A$^{3\mathrm{X}4}$			5.402	5.281	
α-Ara$f$-A$^{2\mathrm{X}5}$					5.220
α-Ara$f$-A$^{3\mathrm{X}5}$					5.271

[a] Measured at 600 MHz on solutions in D_2O at 27° (internal acetone, δ 2.225). [b] The Xyl$p$ residue in the reducing position is denoted **1**, etc.; 2_α and 2_β mean that Xyl$p$-1 is α or β, Ara$f$-A$^{2\mathrm{X}3}$ means arabinofuranose linked to O-2 of Xyl$p$-3, etc., Xyl$p$-3$^{\mathrm{I}}$ means Xyl$p$-3 branched at O-2, Xyl$p$-3$^{\mathrm{II}}$ means Xyl$p$-3 branched at O-3, Xyl$p$-3$^{\mathrm{III}}$ means Xyl$p$-3 branched at O-2,3. [c] Key: ●, Xyl$p$; ◇, α-Ara$f$; ●–●, β-Xyl$p$-(1 → 4)-Xyl$p$; ◇⎺, α-Ara$f$-(1 → 2)-β-Xyl$p$; ◇⁄●, α-Ara$f$-(1 → 3)-β-Xyl$p$.

related feruloylated compound [5-*O*-(*trans*-feruloyl)-α-L-Ara$f$]-(1 → 3)-β-D-Xyl$p$-(1 → 4)-D-Xyl$p$)[9,10], the structure shown was assigned to **3.2**. The ^{1}H NMR data are recorded in Table III.

$$
\begin{array}{ccc}
2^{\mathrm{II}} & & 1 \\
\beta\text{-Xyl}p\text{-}(1 \to 4)\text{-Xyl}p \\
\diagup \\
\alpha\text{-Ara}f\text{-}(1 \to 3) \\
\mathbf{A}^{3\mathrm{X}2}
\end{array}
$$

3.2

Specific assignment of the α-Ara$f$ H-5*proR*,5*proS* signals is based on their relative chemical shifts ($\delta_{5proR} > \delta_{5proS}$) supported by the $J_{4,5}$ values ($J_{4,5proR} < J_{4,5proS}$)[23]. Owing to the presence of a reducing residue, there is an anomeric effect
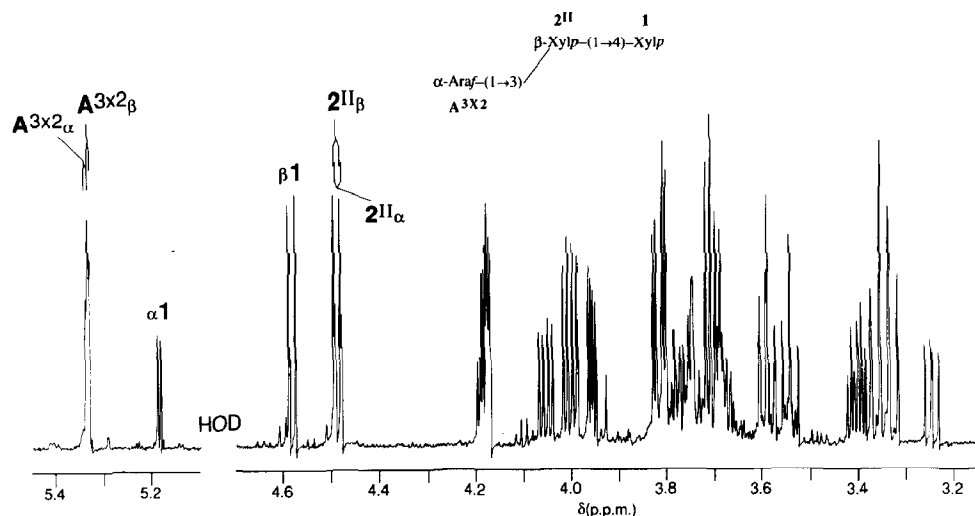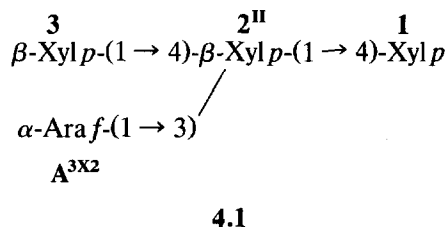
Fig. 3. Resolution-enhanced 600-MHz ^{1}H NMR spectrum of fraction **3.2**. The numbers and letters in the spectrum refer to the corresponding residues in the structure.

with doubling of the H-1,2,3,4 signals of β-Xyl$p$-2^{II} and the H-1 of (1 → 3)-linked α-Ara$f$-A^{3X2}.
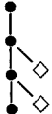
Fraction **4.1**.—The intensities of the H-1 signals for **4.1** (Fig. 4) indicated an arabinosylxylotriose with the Xyl$p$ units β ($J_{1,2}$ 7–8 Hz) and the Ara$f$ unit α ($J_{1,2}$ ~ 1 Hz). Comparison of the ^{1}H NMR data (Table III) with those[12] for AX-31 [β-Xyl$p$-4-(α-Ara$f$-A^{3X3})β-Xyl$p$-3^{II}-β-Xyl$p$-2-Xyl$p$-1] shows that the β-Xyl$p$-4-(α-Ara$f$-A^{3X3})β-Xyl$p$-3^{II} moiety is also part of **4.1**, denoted β-Xyl$p$-3-(α-Ara$f$-A^{3X2})β-Xyl$p$-2^{II}. However, the H-1 resonance (δ 4.509) of β-Xyl$p$-2^{II} of **4.1** has shifted slightly upfield (0.005 ppm), and the resonances of H-1,2,3 of β-Xyl$p$-2^{II} and H-1 of α-Ara$f$-A^{3X2} are double due to an anomeric effect, which accords with the linkage of the α-Ara$f$-(1 → 3)[β-Xyl$p$-(1 → 4)]-β-Xyl$p$ group to a reducing xylose residue in **4.1**.

<pre>
    3   2^{II} 1
β-Xylp-(1 → 4)-β-Xylp-(1 → 4)-Xylp
                     /
 α-Araf-(1 → 3)
    A^{3X2}
</pre>

4.1

Comparison of the ^{1}H NMR data (Table III) of **4.1** and **3.2** shows significant downfield shifts of the α-Ara$f$-A^{3X2} H-1,4,5*proS* signals and significant upfield shifts of the H-2,3,5*proR* signals, reflecting the effect of the change of the terminal α-Ara$f$-(1 → 3)-β-Xyl$p$ group to an α-Ara$f$-(1 → 3)[β-Xyl$p$-(1 → 4)]-β-Xyl$p$ unit. The feruloylated compound β-D-Xyl$p$-(1 → 4)-[5-*O*-(*trans*-feruloyl)-α-L-Ara$f$-(1 →
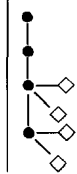
TABLE III

^{1}H NMR data on fractions from Table I

Compound[a]	Residue[a]	Chemical shift[b]					
		H-1	H-2	H-3	H-4	H-5seq/H-5$proR$	H-5ax/H-5$proS$
3.2	α-Xyl$p$-1	5.185	3.545	3.545	3.73 — 3.82	4.055	3.377
	β-Xyl$p$-1	4.584	3.250				
	β-Xyl$p$-2$^{II}_{\beta}$	4.487	3.413	3.594	3.781	4.004	3.340
	β-Xyl$p$-2$^{II}_{\beta}$	4.490	3.403	3.591	3.692 / 3.690		
	α-Ara$f$-A$^{3X2}_{\alpha}$	5.335	4.175	3.959	4.185	3.817	3.705
	α-Ara$f$-A$^{3X2}_{\beta}$	5.332					
4.1	α-Xyl$p$-1	5.185	3.545	3.544	3.73 — 3.82	4.054	3.375
	β-Xyl$p$-1	4.583	3.249		3.771	4.124	3.400
	β-Xyl$p$-2$^{II}_{\alpha}$	4.507	3.348	3.749	3.829		
	β-Xyl$p$-2$^{II}_{\beta}$	4.509	3.440	3.746			
	β-Xyl$p$-3	4.442	3.245	3.414	3.595	3.912	3.278
	α-Ara$f$-A$^{3X2}_{\alpha}$	5.400	4.158	3.903	4.272	3.796	3.714
	α-Ara$f$-A$^{3X2}_{\beta}$	5.395					
5.1	α-Xyl$p$-1	5.183	3.546	3.546	3.73 — 3.82	4.050	3.376
	β-Xyl$p$-1	4.584	3.249				
	β-Xyl$p$-2$_{\alpha}$	4.465	3.298	3.558	3.771	4.140	3.416
	β-Xyl$p$-2$_{\beta}$	4.467	3.290		3.792		
	β-Xyl$p$-3^{III}	4.596	3.539	3.689	3.724	4.023	3.344
	α-Ara$f$-A^{2X3}	5.238	4.151	3.956	4.132	3.816	3.720
	α-Ara$f$-A^{3X3}	5.246	4.175	3.973	4.198	3.813	3.706
5.2	α-Xyl$p$-1	5.186	3.547	3.546	3.73 — 3.82	4.055	3.377
	β-Xyl$p$-1	4.584	3.251				
	β-Xyl$p$-2$^{II}_{\alpha}$	4.507	3.451	3.745	3.781	4.126	3.401
	β-Xyl$p$-2$^{II}_{\beta}$	4.510	3.443		3.837		
	β-Xyl$p$-3^{II}	4.475	3.400	3.581	3.663	3.948	3.312
	α-Ara$f$-A$^{3X2}_{\alpha}$	5.396	4.159	3.902	4.270	3.796	3.715
	α-Ara$f$-a$^{3X2}_{\beta}$	5.391					
	α-Ara$f$-A^{3X3}	5.328	4.175	3.959	4.182	3.817	3.704

6.2

α-Xylp-1	5.186	3.547	3.545	3.781	4.054	3.377
β-Xylp-1	4.584	3.251	3.740	3.836	4.123	3.399
β-Xylp-2$_\alpha^{II}$	4.507	3.448 }				
β-Xylp-2$_\beta^{II}$	4.510	3.440				
β-Xylp-3^{II}	4.489	3.430	3.735	3.793	4.068	3.366
β-Xylp-4	4.432	3.237	3.409	3.591	3.907	3.269
α-Araf-A^{3X2}	5.391 }					
α-Araf-A$_\beta^{3X2}$	5.386	4.161	3.914	4.272	3.800	3.719
α-Araf-A^{3X3}	5.398	4.157	3.900	4.272	3.794	3.715

(header spanning: 3.73 — 3.82)

6.3

α-Xylp-1	5.184	3.545	3.544	3.770	4.049	3.373
β-Xylp-1	4.584	3.249	3.764 }			
β-Xylp-2$_\alpha^{II}$	4.494	3.448	3.761 }	3.830	4.136	3.455
β-Xylp-2$_\beta^{II}$	4.496	3.440				
β-Xylp-3^{III}	4.563	3.536	3.67	3.68	4.056	3.309
α-Araf-A^{3X2}	5.427 }					
α-Araf-A$_\beta^{3X2}$	5.422	4.158	3.911	4.307	3.816	3.728
α-Araf-A^{2X3}	5.244	4.150	3.973	4.15	3.839	3.745
α-Araf-A^{3X3}	5.244	4.174	3.973	4.196	3.811	3.704

(header spanning: 3.73 — 3.82)

7.1

α-Xylp-1	5.184	3.545	3.546	3.772	4.051	3.376
β-Xylp-1	4.584	3.248	3.561	3.792	4.143	3.417
β-Xylp-2$_\alpha$	4.467	3.298 }				
β-Xylp-2$_\beta$	4.467	3.290				
β-Xylp-3^{III}	4.639	3.572	3.828	3.878	4.146	3.431
β-Xylp-4^{II}	4.467	3.409	3.582	3.667	3.956	3.307
α-Araf-A^{2X3}	5.225	4.148	3.958	4.127	3.817	3.720
α-Araf-A^{3X3}	5.271	4.164	3.932	4.301	3.796	3.720
α-Araf-A^{3X4}	5.331	4.175	3.958	4.186	3.815	3.704

(header spanning: 3.73 — 3.82)

TABLE III (continued)

Compound [a]	Residue [a]	Chemical shift [b]					
		H-1	H-2	H-3	H-4	H-5eq /H-5proR	H-5ax /H-5proS
	α-Xylp-1	5.184	3.544	3.545	3.771	4.051	3.376
8.2	β-Xylp-1	4.584	3.247	3.558	3.782	4.139	3.415
	β-Xylp-2α	4.464	3.297 ⎤	←— 3.73 – 3.82 —→			
	β-Xylp-2β	4.466	3.288 ⎦				
	β-Xylp-3[III]	4.626	3.565	3.85	3.86	4.139	3.491
	β-Xylp-4[III]	4.548	3.546	3.669	3.689	3.959	3.302
	α-Araf-A[2X3]	5.221	4.152	3.957	4.125	3.816	3.720
	α-Araf-A[3X3]	5.293	4.163	3.939	4.338	3.826	3.737
	α-Araf-A[2X4]	5.254	4.149	3.973	4.16	3.838	3.737
	α-Araf-A[3X4]	5.246	4.175	3.973	4.198	3.811	3.704

[a] See Table II for the key. [b] In ppm relative to the signal of internal sodium 4,4-dimethyl-4-silapentane-1-sulfonate (using internal acetone at δ 2.225) in D_2O at 27°, acquired at 600 MHz.

Fig. 4. Resolution-enhanced 600-MHz ^{1}H NMR spectrum of fraction **4.2**. The numbers and letters in the spectrum refer to the corresponding residues in the structure.

3)]-β-D-Xyl$p$-(1 → 4)-D-Xyl$p$ has been described[10,24], and the reported ^{1}H NMR assignments accorded those of comparable residues in **4.1**.

Fraction **5.1**.—The intensities of the H-1 signals for **5.1** (Fig. 5) indicated a single diarabinosylxylotriose with the Xyl$p$ units β ($J_{1,2}$ 7–8 Hz) and the Ara$f$ units α ($J_{1,2}$ 1–1.5 Hz). On the various H-1 tracks of the constituent monosaccharides in the 2D HOHAHA spectrum, the total scalar-coupled network for each residue was observed, and the data obtained are summarised in Table III. The observed ROEs along the H-1 tracks in the ROESY spectrum are compiled in Table IV. The ROEs between H-1 of β-Xyl$p$-(**n**) and H-4,5eq of β-Xyl$p$-(**n** − **1**),

Fig. 5. Resolution-enhanced 600-MHz ^{1}H NMR spectrum of fraction **5.1**. The numbers and letters in the spectrum refer to the corresponding residues in the structure.

TABLE IV

Cross-peaks observed at the H-1 tracks in the ROESY spectra of arabinoxylan oligosaccharides, measured with a mixing time of 200 ms

Compound	Residue	ROE effect
5.1	Xyl-2 H-1	Xyl-2 H-3,5ax, Xyl-1β H-4,5eq, Xyl-1α H-4,5
	Xyl-3^{III} H-1	Xyl-3^{III} H-3,5ax, Xyl-2 H-4,5eq
	Ara-A^{2X3} H-1	Ara-A^{2X3} H-2, Ara-A^{3X3} H-2, Xyl-3^{III} H-2
	Ara-A^{3X3} H-1	Ara-A^{3X3} H-2, Ara-A^{2X3} H-2, Xyl-3^{III} H-3
5.2	Xyl-2^{II} H-1	Xyl-2^{II} H-3,5ax, Xyl-1β H-4
	Xyl-3^{II} H-1	Xyl-3^{II} H-3,5ax, Xyl-2^{II} H-4,5,eq
	Ara-A^{3X2} H-1	Ara-A^{3X2} H-2, Xyl-2^{II} H-3
	Ara-A^{3X3} H-1	Ara-A^{3X3} H-2, Xyl-3^{II} H-3
6.3	Xyl-2^{II} H-1	Xyl-2^{II} H-3,5ax, Xyl-1β H-4,5eq, Xyl-1α H-5
	Xyl-3^{III} H-1	Xyl-3^{III} H-3,5ax, Xyl-2^{II} H-4,5eq
	Ara-A^{3X2} H-1	Ara-A^{3X2} H-2, Xyl-2^{II} H-3
	Ara-A^{2X3} H-1	Ara-A^{2X3} H-2, Ara-A^{3X3} H-2 [a], Xyl-3^{III} H-2
	Ara-A^{3X3} H-1	Ara-A^{3X3} H-2, Ara-A^{2X3} H-2 [a], Xyl-3^{III} H-3
7.1	Xyl-2 H-1	Xyl-2 H-3,5ax, Xyl-1β H-4, Xyl-1α H-4,5
	Xyl-3^{III} H-1	Xyl-3^{III} H-3(weak),5ax, Xyl-2 H-4,5eq
	Xyl-4^{II} H-1	Xyl-4^{II} H-3,5ax, Xyl-3^{III} H-4,5eq
	Ara-A^{2X3} H-1	Ara-A^{2X3} H-2, Ara-A^{3X3} H-2, Xyl-3^{III} H-2
	Ara-A^{3X3} H-1	Ara-A^{3X3} H-2, Ara-A^{2X3} H-2, Xyl-3^{III} H-3
	Ara-A^{3X4} H-1	Ara-A^{3X4} H-2(very weak), Xyl-4^{II} H-3
8.2	Xyl-2 H-1	Xyl-2 H-3(weak),5ax, Xyl-1β H-4,5eq, Xyl-1α H-5
	Xyl-3^{III} H-1	Xyl-3^{III} H-3,5ax, Xyl-2 H-4,5eq
	Xyl-4^{III} H-1	Xyl-4^{III} H-3,5ax, Xyl-3^{III} H-4,5eq
	Ara-A^{2X3} H-1	Ara-A^{2X3} H-2, Ara-A^{3X3} H-2, Xyl-3^{III} H-2
	Ara-A^{3X3} H-1	Ara-A^{3X3} H-2(weak), Ara-A^{2X3} H-2, Xyl-3^{III} H-3
	Ara-A^{2X4} H-1	Ara-A^{2X4} H-2, Ara-A^{3X4} H-2, Xyl-4^{III} H-2
	Ara-A^{3X4} H-1	Ara-A^{3X4} H-2(weak), Ara-A^{2X4} H-2, Xyl-4^{III} H-3

[a] Due to the overlap of the H-1 resonances of A^{2X4} and A^{3X4}, the presence of these inter-residual ROE contacts could not be proved unambiguously, but were assumed to be present according to the structure **5.1**.

together with the connectivities α-Ara$f$-A^{2X3}H-1,β-Xyl$p$-3^{III} H-2 and α-Ara$f$-A^{3X3}H-1,β-Xyl$p$-3^{III}H-3 established the sequence in **5.1**.

$$3^{III} \qquad\qquad 2 \qquad\qquad 1$$
$$\beta\text{-Xyl}\,p\text{-}(1 \rightarrow 4)\text{-}\beta\text{-Xyl}\,p\text{-}(1 \rightarrow 4)\text{-Xyl}\,p$$

α-Ara$f$-(1 → 3)

A^{3X3} α-Ara$f$-(1 → 2)

A^{2X3}

5.1

Comparison of the ^{1}H NMR data for **5.1** with those[12] of **AX-33** [β-Xyl$p$-4-(α-Ara$f$-A^{2X3})(α-Ara$f$-A^{3X3})β-Xyl$p$-3^{III}-β-Xyl$p$-2-Xyl$p$-1] shows significant upfield shifts of all the signals of β-Xyl$p$-3^{III} in **5.1** and there are differences in chemical
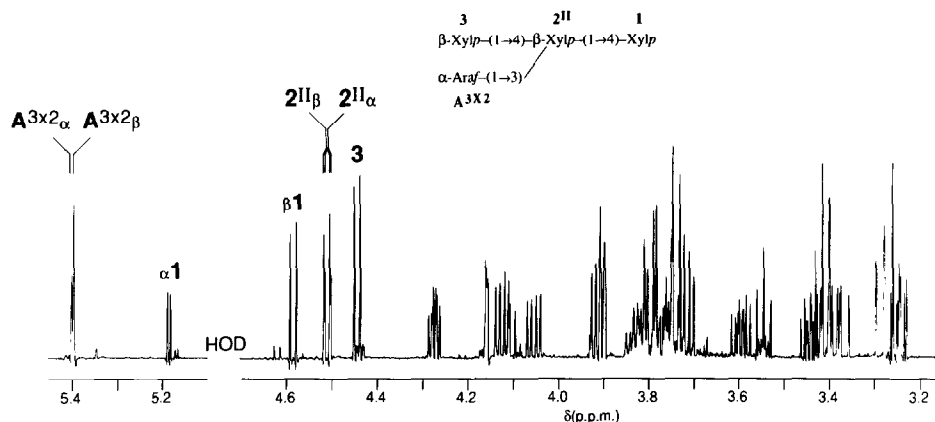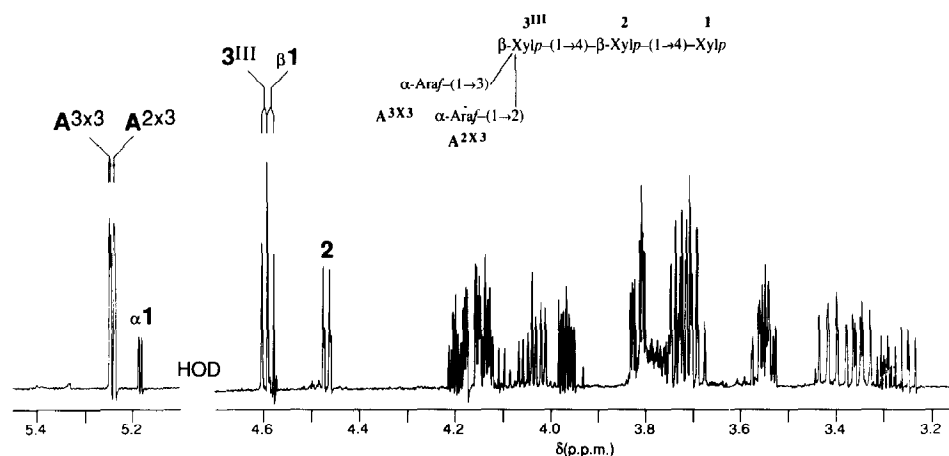
Fig. 6. Resolution-enhanced 600-MHz ^{1}H NMR spectrum of fraction **5.2**. The numbers and letters in the spectrum refer to the corresponding residues in the structure.
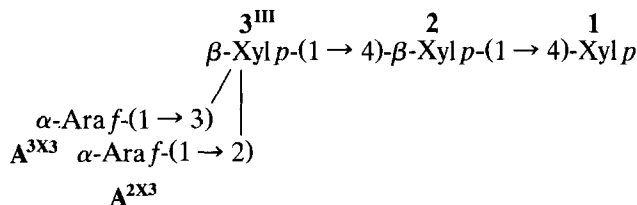
shifts of the signals of the α-Ara$f$ residues. The signals of α-Ara$f$-A^{3X3} are shifted in the same manner as found for α-Ara$f$-A^{3X2} on going from **4.1** to **3.2**. For α-Ara$f$-A^{2X3}, only the H-1 resonance shows a small downfield shift (0.014 ppm), as compared to the same residue in **AX-33**. The inter-residual connectivities A^{2X3}-H-1,A^{3X3}-H-2 and A^{3X3}-H-1,A^{2X3}-H-2, found[12] for **AX-33**, were also present in the ROESY spectrum of **5.1**, but with lower intensities.

Fraction 5.2.—The intensities of the H-1 signals for **5.2** (Fig. 6) indicated a diarabinosylxylotriose. The connectivities were determined as for **5.1** and the data are summarised in Tables III and IV. The ROEs between H-1 of β-Xyl$p$-(**n**) and H-4,5eq of β-Xyl$p$-(**n** − 1), together with the connectivities α-Ara$f$-A^{3X2}H-1,β-Xyl$p$-2^{II}H-3 and α-Ara$f$-A^{3X3}H-1,β-Xyl$p$-3^{II}H-3 established the sequence in **5.2**.

$$
\begin{array}{l}
\quad\quad A^{3X3} \\
\alpha\text{-Ara}f\text{-}(1 \rightarrow 3) \\
\quad\quad\quad\quad\quad \diagdown \\
\quad\quad\quad\quad\quad\quad 3^{II} \quad\quad\quad\quad\quad 2^{II} \quad\quad\quad\quad 1 \\
\quad\quad\quad\quad\quad \beta\text{-Xyl}p\text{-}(1 \rightarrow 4)\text{-}\beta\text{-Xyl}p\text{-}(1 \rightarrow 4)\text{-Xyl}p \\
\quad\quad\quad\quad\quad\quad\quad\quad\quad\quad \diagup \\
\quad\quad\quad\quad \alpha\text{-Ara}f\text{-}(1 \rightarrow 3) \\
\quad\quad\quad\quad\quad\quad A^{3X2}
\end{array}
$$

5.2

Comparison of the ^{1}H NMR data for **5.2** with those[13] of **AX-41** [β-Xyl$p$-5-(α-Ara$f$-A^{3X4})β-Xyl$p$-4^{II}-(α-Ara$f$-A^{3X3})β-Xyl$p$-3^{II}-β-Xyl$p$-2-Xyl$p$-1] shows large upfield shifts for all signals derived from β-Xyl$p$-3^{II} relative to those of β-Xyl$p$-4^{II} of **AX-41**, as expected on going from an internal to a terminal residue. The significant upfield shifts of the α-Ara$f$-A^{3X3} H-1,4,5$proS$ signals and downfield
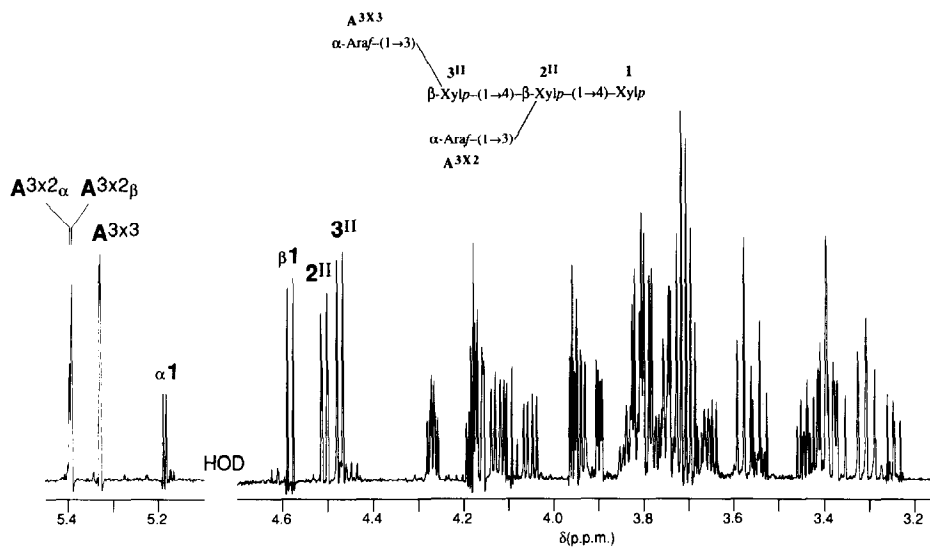
Fig. 7. Resolution-enhanced 600-MHz ^{1}H NMR spectrum of fraction **6.2**. The numbers and letters in the spectrum refer to the corresponding residues in the structure.

shifts of the H-2,3,5*proR* signals in **5.2**, relative to the same signals of α-Ara$f$-A^{3X4} in **AX-41**, is noteworthy. Similar differences in chemical shifts were found for α-Ara$f$-A^{3X2} in **3.2** and **4.1** (see above). The ^{1}H NMR data of α-Ara$f$-A^{3X3} in **5.2** and of α-Ara$f$-A$^{3X2}\beta$ in **3.2** are (almost) identical.

Fraction **6.1**.—The intensities of the H-1 signals for **6.1** indicated a diarabinosylxylotetraose. The chemical shift data matched exactly those[12] of **AX-33** and the chemical shifts of the H-1 resonances are summarised in Table II.

$$\begin{array}{cccc}
\textbf{4} & \textbf{3}^{\textbf{III}} & \textbf{2} & \textbf{1}
\end{array}$$
β-Xyl$p$-(1 → 4)-β-Xyl$p$-(1 → 4)-β-Xyl$p$-(1 → 4)-Xyl$p$

$\qquad\qquad\qquad$ /|

$\qquad \alpha$-Ara$f$-(1 → 3) $\quad$|

A^{3X3} $\quad \alpha$-Ara$f$-(1 → 2)

$\qquad\qquad$ A^{2X3}

<div align="center">

6.1

</div>

Compound **6.1** was also formed on enzymic treatment of barley flour[11].

Fraction **6.2**.—The intensities of the H-1 signals for **6.2** (Fig. 7) indicated a diarabinosylxylotetraose. The connectivities were determined as for **5.1** and the data obtained are summarised in Table III. The ^{1}H NMR data that reflect[13] the presence of the terminal β-Xyl$p$-5-(α-Ara$f$-A^{3X4})β-Xyl$p$-4$^{\text{II}}$-(α-Ara$f$-A^{3X3})β-Xyl$p$-3$^{\text{II}}$ moiety in **AX-41** are also found for **6.2** and are assigned to β-Xyl$p$-4-(α-Ara$f$-A^{3X3})β-Xyl$p$-3$^{\text{II}}$-(α-Ara$f$-A^{3X2})β-Xyl$p$-2$^{\text{II}}$ and a reducing xylose residue. The finding of anomeric effects on the resonance of α-Ara$f$-A^{3X2} H-1 and β-Xyl$p$-2$^{\text{II}}$ H-1,2 and a small upfield shift (δ 4.510) of the resonance of β-Xyl$p$-2$^{\text{II}}_\beta$ H-1,
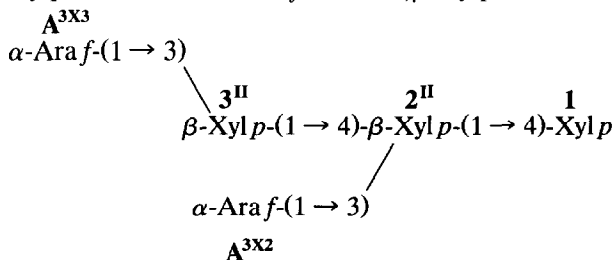
Fig. 8. Resolution-enhanced 600-MHz ^{1}H NMR spectrum of fraction **6.3**. The numbers and letters in the spectrum refer to the corresponding residues in the structure.

compared to that (δ 4.514) of the β-Xyl$p$-3^{II} H-1 resonance in **AX-41**, supports this conclusion (see also β-Xyl$p$-2^{II} of **4.1** and **5.2**) and the structure assigned.

$$\mathbf{A}^{3X3}$$
$$\alpha\text{-Ara}\,f\text{-}(1 \to 3)$$

$$\mathbf{4} \qquad\qquad\qquad \searrow 3^{II} \qquad\qquad\qquad 2^{II} \qquad\qquad\qquad \mathbf{1}$$
$$\beta\text{-Xyl}\,p\text{-}(1 \to 4)\text{-}\beta\text{-Xyl}\,p\text{-}(1 \to 4)\text{-}\beta\text{-Xyl}\,p\text{-}(1 \to 4)\text{-Xyl}\,p$$

$$\nearrow$$
$$\alpha\text{-Ara}\,f\text{-}(1 \to 3)$$
$$\mathbf{A}^{3X2}$$

6.2

Fraction **6.3**.—The intensities of the H-1 signals for **6.3** (Fig. 8) indicated a triarabinosylxylotriose. The connectivities were established as for **5.1** and the data obtained are summarised in Tables III and IV. The ROEs between H-1 of β-Xyl$p$-(**n**) and H-4,5eq of β-Xyl$p$-(**n** − **1**), together with the connectivities α-Ara$f$-$\mathbf{A}^{3X2}$ H-1,β-Xyl$p$-2^{II} H-3, α-Ara$f$-$\mathbf{A}^{2X3}$ H-1,β-Xyl$p$-3^{III} H-2 and α-Ara$f$-$\mathbf{A}^{3X3}$ H-1,β-Xyl$p$-3^{III} H-3 established the sequence in **6.3**.

$$\mathbf{A}^{2X3}$$
$$\mathbf{A}^{3X3} \quad \alpha\text{-Ara}\,f\text{-}(1 \to 2)$$
$$\alpha\text{-Ara}\,f\text{-}(1 \to 3) \quad \Big|$$
$$\searrow 3^{III} \qquad\qquad 2^{II} \qquad\qquad\qquad \mathbf{1}$$
$$\beta\text{-Xyl}\,p\text{-}(1 \to 4)\text{-}\beta\text{-Xyl}\,p\text{-}(1 \to 4)\text{-Xyl}\,p$$

$$\nearrow$$
$$\alpha\text{-Ara}\,f\text{-}(1 \to 3)$$
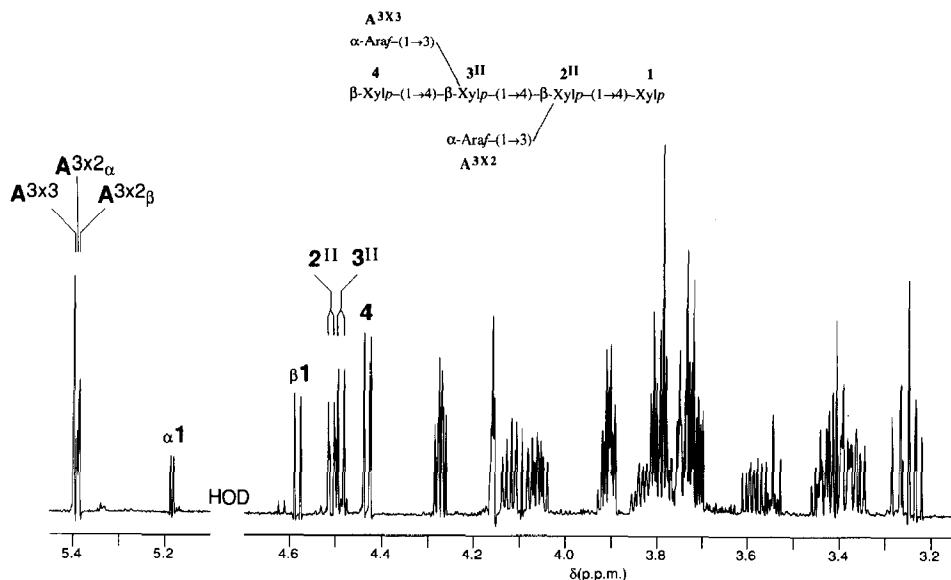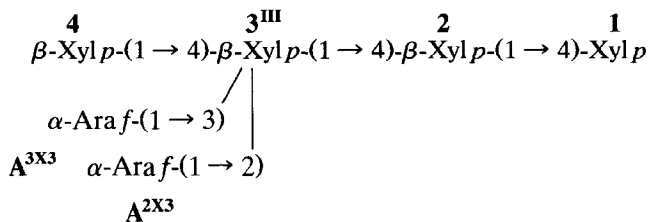$$\mathbf{A}^{3X2}$$

6.3

Fig. 9. Resolution-enhanced 600-MHz ^{1}H NMR spectrum of fraction **7.1**. The numbers and letters in the spectrum refer to the corresponding residues in the structure.

Owing to overlap of the H-1 resonances of α-Araf-A^{2X3} and α-Araf-A^{3X3}, two sets of signals were observed along the HOHAHA H-1 track at δ 5.244. One set of signals match those of α-Araf-A^{3X3} of **5.1** and were assigned to the corresponding residue in **6.3**. Owing to overlap of the α-Araf-A^{2X3} H-2,4 signals, the chemical shift of the H-4 resonance could not be determined accurately. An anomeric effect was observed on the signals for β-Xylp-2^{II} H-1,2,3 and α-Araf-A^{3X2} H-1, corroborating the structure assigned.

Fraction **7.1**.—The intensities of the H-1 signals for **7.1** (Fig. 9) indicated a triarabinosylxylotetraose as the major compound. The connectivities were established as for **5.1** and the data obtained are summarised in Tables III and IV. The ROEs between H-1 of β-Xylp-(**n**) and H-4,5eq of β-Xylp-(**n** − **1**), together with the connectivities α-Araf-A^{2X3} H-1,β-Xylp-3^{III} H-2, α-Araf-A^{3X3} H-1,β-Xylp-3^{III} H-3, and α-Araf-A^{3X4} H-1,β-Xylp-4^{II} H-3 established the sequence in **7.1**.

A^{3X4}
α-Araf-(1 → 3)
　　　　　　＼　4^{II}　　　　3^{III}　　　　　　2　　　　　　　1
　　　　　　β-Xylp-(1 → 4)-β-Xylp-(1 → 4)-β-Xylp-(1 → 4)-Xylp
　　　　　　　　　　　　　／|
　　　　　α-Araf-(1 → 3)　|
　　　A^{3X3}　　α-Araf-(1 → 2)
　　　　　　　　A^{2X3}

7.1

Owing to the overlap of the H-1 signals of β-Xyl$p$-2 and β-Xyl$p$-4^{II}, two sets of signals were observed along the HOHAHA H-1 track at δ 4.467. Besides the ROEs mentioned above, the ROESY spectrum shows also the inter-residual connectivities A^{2X3}-H-1,A^{3X3}-H-2 and A^{3X3}-H-1,A^{2X3}-H-2, characteristic for the 2,3-substitution of a $(1 \rightarrow 4)$-linked β-Xyl$p$ residue by two terminal α-Ara$f$ groups[12,13]. Comparison of the ^{1}H NMR data of **7.1** with those[13] of **AX-54c** [β-Xyl$p$-5-(α-Ara$f$-A^{3X4})β-Xyl$p$-4^{II}-(α-Ara$f$-A^{2X3})(α-Ara$f$-A^{3X3})β-Xyl$p$-3^{III}-β-Xyl$p$-2-Xyl$p$-1] shows a good match for the resonances of β-Xyl$p$-1,2,3^{III} and α-Ara$f$-A^{2X3} and only small deviations for those of α-Ara$f$-A^{3X3}, in particular H-3,5$proR$,5$proS$. The structural change in the non-reducing terminal part on going from **7.1** to **AX-54c** is reflected by the large upfield shifts for all signals of β-Xyl$p$-4^{II}. The ^{1}H NMR data of α-Ara$f$-A^{3X4} in **7.1** match those for α-Ara$f$-A^{3X2}_{β} in **3.2** and α-Ara$f$-A^{3X3} in **5.2**, and support the structure assigned.

Fraction **8.1**.—The intensities of the H-1 signals for **8.1** indicated a triarabinosylxylopentaose. The chemical shift data match exactly those[13] of **AX-54c**, and the chemical shifts of the H-1 resonances are summarised in Table II.

$$A^{3X4}$$
$$\alpha\text{-Ara}\,f\text{-}(1 \rightarrow 3)$$
$$\begin{array}{ccccc} 5 & \diagdown\;4^{II} & 3^{III} & 2 & 1 \\ \beta\text{-Xyl}\,p\text{-}(1 \rightarrow 4)\text{-}\beta\text{-Xyl}\,p\text{-}(1 \rightarrow 4)\text{-}\beta\text{-Xyl}\,p\text{-}(1 \rightarrow 4)\text{-}\beta\text{-Xyl}\,p\text{-}(1 \rightarrow 4)\text{-Xyl}\,p \end{array}$$
$$\alpha\text{-Ara}\,f\text{-}(1 \rightarrow 3)$$
$$A^{3X3}\quad \alpha\text{-Ara}\,f\text{-}(1 \rightarrow 2)$$
$$A^{2X3}$$

8.1

Fraction **8.2**.—The intensities of the H-1 signals for **8.2** (Fig. 10) indicated a tetra-arabinosylxylotetraose. The connectivities were established as for **5.1** and the data are summarised in Tables III and IV. The ROEs between H-1 of β-Xyl$p$-(**n**) and H-4,5eq of β-Xyl$p$-(**n** − 1), together with the connectivities α-Ara$f$-A^{2X3} H-1,β-Xyl$p$-3^{III} H-2, α-Ara$f$-A^{3X3} H-1,β-Xyl$p$-3^{III} H-3, α-Ara$f$-A^{2X4} H-1,β-Xyl$p$-4^{III} H-2, and α-Ara$f$-A^{3X4} H-1,β-Xyl$p$-4^{III} H-3 establish the sequence in **8.2**.

$$A^{2X4}$$
$$A^{3X4}\quad \alpha\text{-Ara}\,f\text{-}(1 \rightarrow 2)$$
$$\alpha\text{-Ara}\,f\text{-}(1 \rightarrow 3)$$
$$\begin{array}{cccc} \diagdown\,4^{III} & 3^{III} & 2 & 1 \\ \beta\text{-Xyl}\,p\text{-}(1 \rightarrow 4)\text{-}\beta\text{-Xyl}\,p\text{-}(1 \rightarrow 4)\text{-}\beta\text{-Xyl}\,p\text{-}(1 \rightarrow 4)\text{-Xyl}\,p \end{array}$$
$$\alpha\text{-Ara}\,f\text{-}(1 \rightarrow 3)$$
$$A^{3X3}\quad \alpha\text{-Ara}\,f\text{-}(1 \rightarrow 2)$$
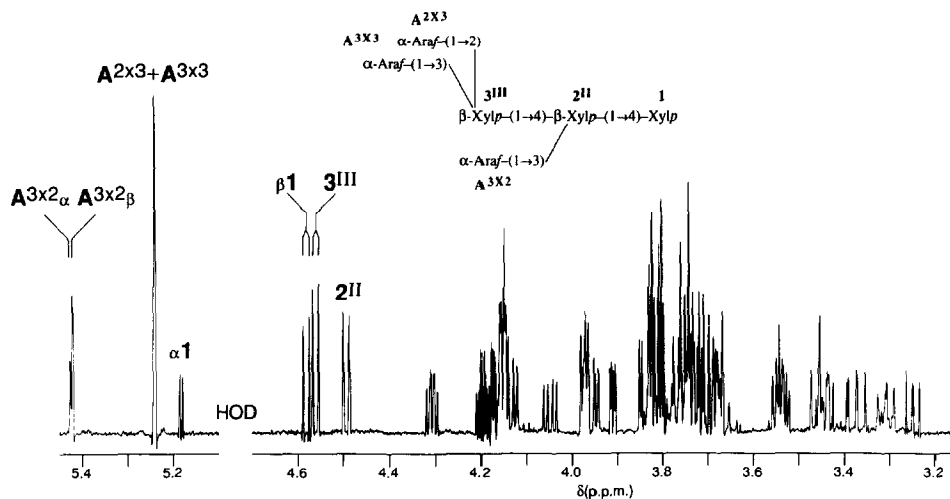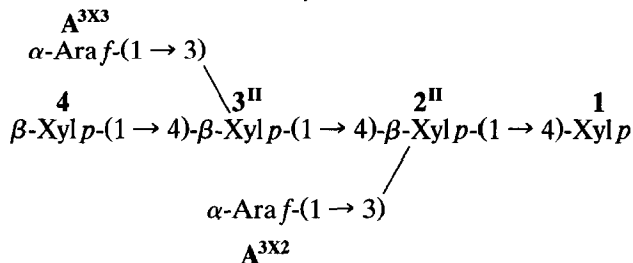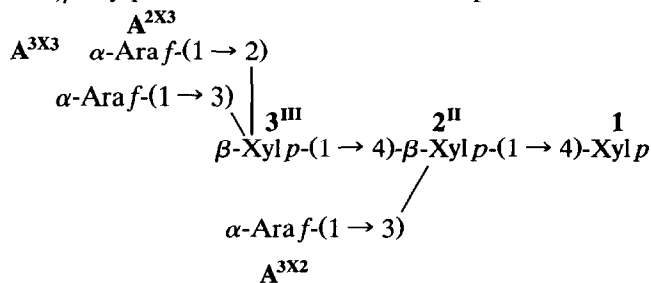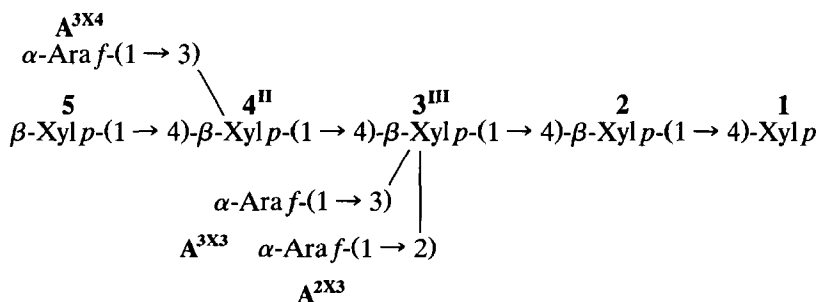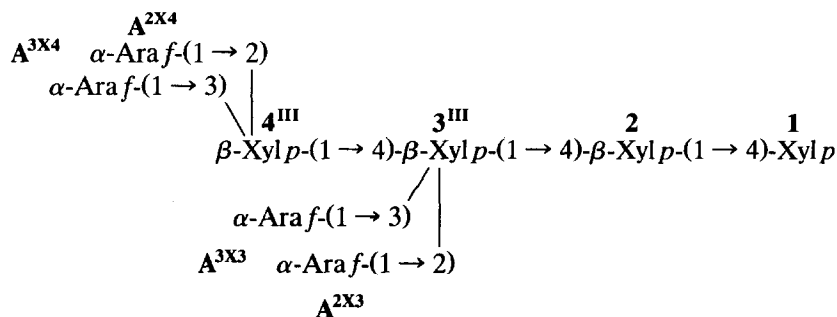$$A^{2X3}$$

8.2

Fig. 10. Resolution-enhanced 600-MHz ^{1}H NMR spectrum of fraction **8.2**. The numbers and letters in the spectrum refer to the corresponding residues in the structure.

The presence of the tetra-arabinosylxylobiose unit in **8.2** is reflected by a characteristic set of four α-Ara$f$ H-1 signals (Table III). The inter-residual α-Ara$f$ H-1,2 connectivities between α-Ara$f$-A^{2X3} and α-Ara$f$-A^{3X3} and between α-Ara$f$-A^{2X4} and α-Ara$f$-A^{3X4} support the presence of two 2,3-branched β-Xyl$p$ residues.

Fraction **9.1**.—The intensities of the H-1 signals for **9.1** indicated a tetra-arabinosylxylopentaose. The chemical shift data match exactly those[13] of **AX-59** and the chemical shifts of the H-1 resonances are summarised in Table II.
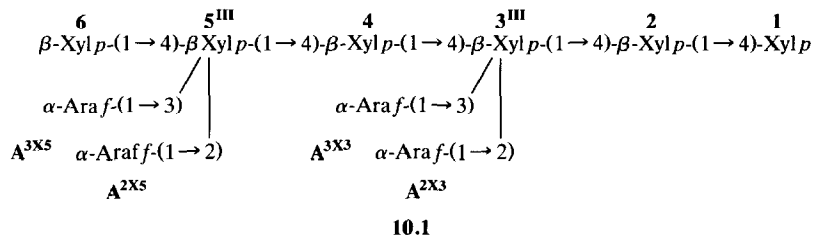
$$
\begin{array}{c}
\qquad\quad \mathbf{A^{2X4}} \\
\mathbf{A^{3X4}} \quad \alpha\text{-Ara}f\text{-}(1 \to 2) \\
\quad \alpha\text{-Ara}f\text{-}(1 \to 3) \qquad\qquad | \\
\quad 5 \qquad\qquad \backslash\; |\, 4^{III} \qquad\quad 3^{III} \qquad\qquad 2 \qquad\qquad 1 \\
\beta\text{-Xyl}p\text{-}(1 \to 4)\text{-}\beta\text{-Xyl}p\text{-}(1 \to 4)\text{-}\beta\text{-Xyl}p\text{-}(1 \to 4)\text{-}\beta\text{-Xyl}p\text{-}(1 \to 4)\text{-Xyl}p \\
\qquad\qquad\qquad\qquad\qquad / \\
\quad\qquad\qquad \alpha\text{-Ara}f\text{-}(1 \to 3) \;| \\
\qquad \mathbf{A^{3X3}} \quad \alpha\text{-Ara}f\text{-}(1 \to 2) \\
\qquad\qquad \mathbf{A^{2X3}}
\end{array}
$$

9.1

The characteristic set of four α-Ara$f$ H-1 and two β-Xyl$p$ H-1 signals, which reflects the presence of an internal $(1 \to 4)$-linked xylobiose unit composed of two 2,3-branched β-Xyl$p$ with four α-Ara$f$ residues, differs significantly from the set for **8.2**.

Fraction **9.2**.—The ^{1}H NMR spectrum of **9.2**, which indicated the presence of at least two components, could not be unravelled due to its complexity. The

presence of a mixture was reflected by the HPAE-PAD chromatogram (Fig. 2) for fraction **9**.

Fraction **10.1**.—The intensities of the H-1 signals for **10.1** indicated a tetra-arabinosylxylohexaose. The chemical shift data match exactly those[13] of **AX-57**[II] and the chemical shifts of the H-1 resonances are summarised in Table II.

$$
\begin{array}{cccccc}
6 & 5^{III} & 4 & 3^{III} & 2 & 1 \\
\beta\text{-Xyl}p\text{-}(1\to4)\text{-}\beta\,\text{Xyl}p\text{-}(1\to4)\text{-}\beta\text{-Xyl}p\text{-}(1\to4)\text{-}\beta\text{-Xyl}p\text{-}(1\to4)\text{-}\beta\text{-Xyl}p\text{-}(1\to4)\text{-Xyl}p
\end{array}
$$

α-Ara f-(1 → 3) α-Ara f-(1 → 3)

A^{3X5} α-Araf f-(1 → 2) A^{3X3} α-Ara f-(1 → 2)

A^{2X5} A^{2X3}

10.1

Thus, of the arabinosylxylose oligosaccharides present in the enzymic digest of an alkali-extractable arabinoxylan from the soft-wheat variety *Arminda*, four (**6.1**, **8.1**, **9.1**, and **10.1**) have been identified also in an enzymic digest of a warm-water-extractable arabinoxylan from *Kadet* wheat flour[12,13]. Comparison of the oligosaccharides obtained in this and the previous studies[12,13] showed remarkable differences. Since, for *Arminda* wheat flour, no major differences in branching pattern between water-extractable and alkali-extractable arabinoxylans were found[16], the differences in the oligosaccharides obtained are likely to reflect differences in enzyme specificity rather than differences in arabinoxylan structure. The patterns of action of various types of endo-(1 → 4)-β-D-xylanases on cereal arabinoxlans are under investigation.

ACKNOWLEDGMENTS

REFERENCES

1 G.B. Fincher and B.A. Stone, *Adv. Cereal Sci. Technol.*, 8 (1986) 207–295.
2 R.A. Hoffmann, M. Roza, J. Maat, J.P. Kamerling, and J.F.G. Vliegenthart, *Carbohydr. Polym.*, 15 (1991) 415–430.
3 C.M. Ewald and A.S. Perlin, *Can. J. Chem.*, 37 (1959) 1254–1259.
4 D.G. Medcalf and K.A. Gilles, *Cereal Chem.*, 45 (1968) 550–556.
5 P. Aman and S. Bengtsson, *Carbohydr. Polym.*, 15 (1991) 405–414.
6 M.M. Smith and R.D. Hartley, *Carbohydr. Res.*, 118 (1983) 65–80.
7 F. Gubler, A.E. Ashford, A. Bacic, A.B. Blakeney, and B.A. Stone, *Aust. J. Plant Physiol.*, 12 (1985) 307–309.

8 H.R. Goldschmid and A.S. Perlin, *Can. J. Chem.*, 41 (1963) 2272–2277.

9 I. Mueller-Harvey, R.D. Hartley, P.J. Harris, and E.H. Curzon, *Carbohydr. Res.*, 148 (1986) 71–85.

10 T. Ishii and T. Hiroi, *Carbohydr. Res.*, 196 (1990) 175–183.

11 K. Bock, J.Ø. Duus, B. Norman, and S. Pedersen, *Carbohydr. Res.*, 211 (1991) 219–233.

12 R.A. Hoffmann, B.R. Leeflang, M.M.J. de Barse, J.P. Kamerling, and J.F.G. Vliegenthart, *Carbohydr. Res.*, 221 (1991) 63–81.

13 R.A. Hoffmann, T. Geijtenbeek, J.P. Kamerling, and J.F.G. Vliegenthart, *Carbohydr. Res.*, 223 (1992) 19–44.

14 H. Gruppen, R.J. Hamer, and A.G.J. Voragen, *J. Cereal Sci.*, 13 (1991) 275–290.

15 H. Gruppen, R.J. Hamer, and A.G.J. Voragen, *J. Cereal Sci.*, (1992) in press.

16 H. Gruppen, R.J. Hamer, and A.G.J. Voragen, *J. Cereal Sci.*, (1992) in press.

17 F.J.M. Kormelink, M.J.F. Searle-vanLeeuwen, T.M. Wood, A.G.J. Voragen, and W. Pilnik, in C. Grassi, G. Gosse, and G. dosSantos (Eds.), *Biomass for Energy and Industry; 5th E.C. Conference*, Elsevier Applied Science, London, 1990, pp. 2.66–2.74.

18 M.T. Tollier and J.P. Robin, *Ann. Technol. Agric.*, 28 (1979) 1–15.

19 H.N. Englyst and J.H. Cummings, *Analyst*, 109 (1984) 937–942.

20 H. Gruppen, J.P. Marseille, A.G.J. Voragen, R.J. Hamer, and W. Pilnik, *J. Cereal Sci.*, 9 (1989) 247–260.

21 J.F.G. Vliegenthart, L. Dorland, and H. van Halbeek, *Adv. Carbohydr. Chem. Biochem.*, 41 (1983) 209–374.

22 K. Mizutani, R. Kasai, M. Nakamura, O. Tanaka, and H. Matsuura, *Carbohydr. Res.*, 185 (1989) 27–38.

23 G.D. Wu, A.S. Serianni, and R. Baker, *J. Org. Chem.*, 48 (1983) 1750–1757.

24 A. Kato, J.-I. Azuma, and T. Koshijima, *Agric. Biol. Chem.*, 51 (1987) 1691–1693.